IEEE Access
Multidisciplinary | Rapid Review | Open Access Journal

Received November 3, 2019, accepted November 19, 2019, date of publication November 25, 2019,
date of current version December 10, 2019.

Digital Object Identifier 10.1109/ACCESS.2019.2955495

A High-Isolation Building Block Using Stable Current Nulls for 5G Smartphone Applications

AIDI REN[1], YING LIU[1], (Senior Member), HONG-WEI YU[1], YONGTAO JIA[1], (Member, IEEE), CHOW-YEN-DESMOND SIM[2], (Senior Member, IEEE), AND YUNXUE XU[1]

[1]Science and Technology on Antenna and Microwave Laboratory, Xidian University, Xi'an 710071, China
[2]Department of Electrical Engineering, Feng Chia University, Taichung 40724, Taiwan

Corresponding author: Ying Liu (liuying@mail.xidian.edu.cn)

This work was supported by the National Natural Science Foundation of China under Grant 61871309 and Grant 61971335.

ABSTRACT In this paper, a new design method to enhance the isolation of a two-antenna building block is introduced. Here, a two-antenna building block (Ant 1 and Ant 2) that is composed of a gap-coupled loop antenna (Ant 1) and a loop antenna (Ant 2) is meticulously designed to allow Ant 1 to excite a standing-wave region that can be formed on the structure of Ant 2. To exhibit high isolation (26 dB) between the two antennas, the stable current null point existed in the standing wave region is exploited and designed to fall at the feed point of Ant 2 during the excitation of Ant 1. By employing this proposed building block, a four-port multiple-input multiple-output (MIMO) system and an eight-port MIMO system operating in the long term evolution (LTE) band 42 (3.4-3.6 GHz) are implemented. The proposed four-antenna and eight-antenna MIMO arrays can yield desirable measured isolation of better than 23 dB and 17.9 dB, respectively, over the band of interest, and their respective measured ECCs (envelope correlation coefficients) were lower than 0.032 and 0.075. To further evaluate the MIMO performances of the presented MIMO arrays, their ergodic channel capacities are also investigated.

INDEX TERMS Fifth-generation (5G) smartphone, multiple-input multiple-output (MIMO), building block, high isolation.

I. INTRODUCTION

The fifth-generation (5G) mobile communication is capable of ultra-fast speeds, low latency and excellent reliability. To meet the 5G requirement of very high capacity, the MIMO technology is widely applied to wireless communication [1]. The identification of the C-band frequency spectrum (3.4-3.6 GHz) for upcoming 5G communication [2] has recently promoted the investigation of integrating sub-6GHz MIMO array with multi-antenna element into a smartphone. However, simultaneously integrating more than 6- or 8-antenna elements into a smartphone remains a challenging target owing to limited clearance zone, not to mention to take into consideration on how to achieve desirable isolation between antenna elements.

In order to realize desirable isolation and envelop correlation coefficient (ECC), recently, many decoupling methods have been reported [3]–[24]. Amid these methods, the neutralization line (NL) method is utilized to yield acceptable isolation between adjacent antennas [3]–[7], however, the obtained isolations of these reported eight-antenna MIMO systems were around 12 dB. Other methods such as the defected ground structure (DGS) technique have also been exploited to enhance the isolation [8], [9], but it is inevitable that the application of the NL or DGS will result in the increased complexity of the MIMO system and the occupied extra spaces. In [10]–[13], even though the diversity techniques have been employed to enhance the isolation, these designs only achieved isolation of around 13 dB. Consequently, to further acquire higher isolation of better than 20 dB and 17 dB, a four-antenna MIMO system and an eight-antenna MIMO system formed by tightly arranged orthogonal mode pairs were respectively investigated in [14].

The associate editor coordinating the review of this manuscript and approving it for publication was Pietro Savazzi.

Besides the decoupling methods mentioned above, many other decoupling technologies have also been reported [15]–[24]. In [15], [16], different array elements were employed to enhance the isolation, but the sizes of their MIMO systems are too large and the obtained isolation is undesirable. In [17], [18], the characteristic mode theory (CMT) was employed to design a MIMO array. The isolation of the 8-antenna MIMO system in [18] was higher than 15 dB. Nevertheless, the works reported in [19]–[21] have exploited the possibilities of not applying any additional external decoupling structure, in which [19], [20] have exhibited isolations higher than 10 dB within a large MIMO size, while [21] has acquired isolation better than 13 dB by selecting optimum distance between the slots of a 4-antenna MIMO array composed of four slots.

The technique of designing a 2-antenna building block was first reported in [22] for an 8-antenna MIMO array, in which the building block was composed of two asymmetrical mirrored gap-coupled loop antennas. Even though the building block has a very compact size, the isolation was only higher than 10 dB with the efficiency between 40% and 52% over the operation bandwidth. To acquire isolation higher than 17.5 dB, [23] has utilized balanced open slot elements for its 8-MIMO array so that balanced slot mode with reduced ground current effect can be excited effectively, thus enhancing the isolation between adjacent elements. However, too much space around the system ground was occupied by the 8-antenna MIMO array.

Recently, the technique of exploiting the stable null-amplitude fields appearing on the ground plane's edges excited by the higher-order modes of an IFA has been studied [24]. Although isolation higher than 25 dB can be attained by placing the other IFAs onto the stable E-field null points, additional external decoupling structures (resonant strip) are still required if a multi-antenna array of more than two antennas is to be realized. Notably, as the number of stable null-amplitude field excited on the ground plane (fit for a smartphone) is limited at 3.5 GHz, therefore, it is difficult to design a MIMO array with more than 8-antenna elements by applying this method.

In this paper, a novel method that exploits the standing-wave region to acquire high isolation is provided. Here, instead of investigating the null-amplitude fields appearing on the ground plane's edges excited by the higher-order modes as in [24], this work has exploited a new standing-wave region by meticulously designing a two-element building block (Ant 1 and Ant 2), in which the standing-wave region excited by Ant 1 can be formed on the structure of Ant 2, and the feed position of Ant 2 should be placed at the stable current null. Because of the existence of a stable current null at the feed point of Ant 2 (during the excitation of Ant 1); the two-antenna building block will exhibit very high isolation. Notably, the two different loop antennas that are selected to form the high-isolation building block have exhibited isolation level of better than 26 dB. Based on this building block structure, a 4 × 4 and 8 × 8 MIMO system operating at LTE band 42 (3.4-3.6 GHz) are designed and investigated. The isolation levels of the four-port and eight-port MIMO system without loading any additional decoupling structure are higher than 23 dB and 17.9 dB, respectively, and their corresponding ECCs are 0.032 and 0.075.

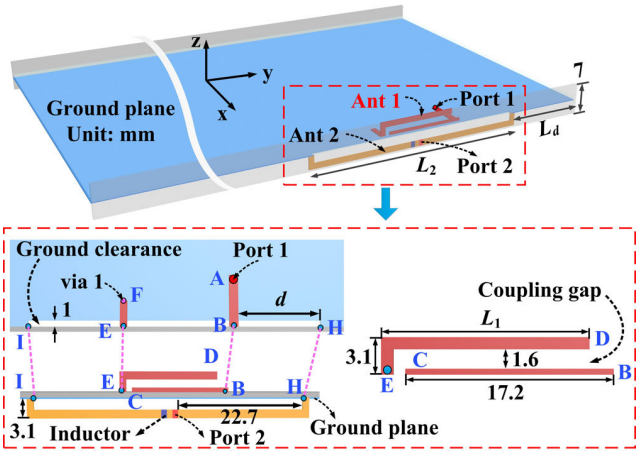

FIGURE 1. Configuration of the high-isolation building block. Ant 1 is a gap-coupled loop antenna and Ant 2 is a loop antenna. $d = 13.7$, $L_d = 16.4$, $L_1 = 16.2$, $L_2 = 48.4$ (Unit: mm).

II. THE HIGH-ISOLATION BUILDING BLOCK

A. GEOMETRY AND PERFORMANCE OF THE HIGH-ISOLATION BUILDING BLOCK

Fig. 1 illustrates the geometrical configuration of the proposed high-isolation building block. An FR4 substrate with volume of 145 mm × 75 mm × 0.8 mm ($\varepsilon_r = 4.4$, $\tan\delta = 0.02$) is selected to be the main system board, and a ground plane is printed on the bottom surface. Here, two vertically standing FR4 side boards each with dimension of 145 mm × 7 mm × 0.8 mm are mounted along the two longer side edges (at the middle) of the main system board, and the proposed building block is printed on the side board.

The detailed dimensions of the proposed high-isolation building block are given in the red dashed area, as described in Fig. 1. Here, the proposed high-isolation building block is comprised of a gap-coupled loop antenna (Ant 1) and a loop antenna (Ant 2), and they are etched on the inner surface (upper and lower half sections) of the side board. Ant 2 is a narrow loop structure HI (of width 1.2 mm, side length 48.4, and side breadth 3.1 mm) printed on the lower half section of the side board, and a chip inductor (9.1 nH) is embedded near to the feeding port of Ant 2 (port 2) for achieving better impedance matching. As for Ant 1, it is composed of a grounded strip DEF, a feeding strip ABC and a coupled gap of 1.6 mm. Ant 1 is fed through port 1 and shorted to the ground through via 1. The strip line AB (1.5 mm × 8 mm) is a 50 Ω microstrip line, while strip line FE (1 mm × 3.2 mm) is for tuning the impedance matching of Ant 1. The two strip lines are located on the top surface of the main system board. It is noteworthy that the width of the ground clearance is only 1 mm (0.012 λ at 3.5 GHz), and it has a length of 48.4 mm.

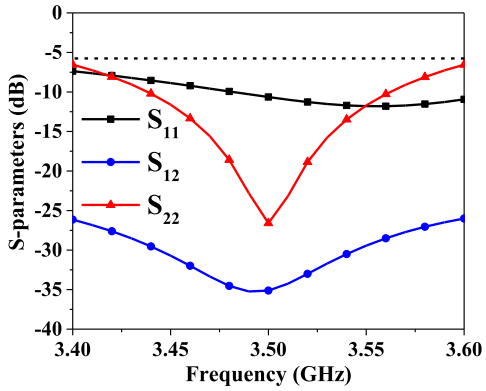

FIGURE 2. Simulated S-parameters of the proposed high-isolation building block.

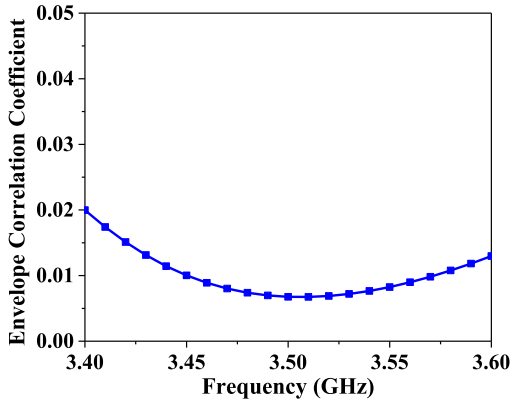

FIGURE 3. Simulated ECC of the presented high-isolation building block.

Fig. 2 illustrates the simulated (via HFSS) S-parameters of the proposed high-isolation building block. In this figure, both Ants 1 and 2 cover the desired 6-dB impedance bandwidth (3.4-3.6 GHz), and despite the close proximity between the two antennas, their corresponding isolation is greater than 26 dB, which is very promising for 5G MIMO system. In terms of MIMO diversity performance, the simulated results presented in Fig. 3 have shown ECC levels lower than 0.02 across the entire band of interest.

According to the above simulated results, the proposed building block can yield desirable isolation (better than 26 dB) and ECC (lower than 0.02), which is very promising for designing multi-antenna systems.

B. DECOUPLING MECHANISM

As reported in [24], two traveling waves propagating in the opposite directions along the edges of the metal ground can be excited by Ant 1. Fig. 4(a) illustrates the two traveling waves and the standing wave region that are excited on the ground plane. In this figure, stable null points are existed in the standing wave region and they can be exploited to arrange other antennas. However, as indicated in [24], the number of the stable null points on the metal ground is limited at 3.5 GHz, and if this method is to be applied

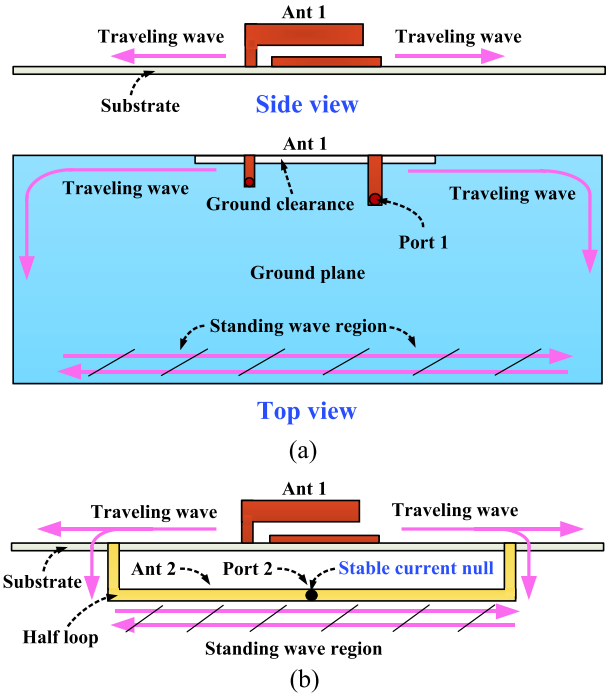

FIGURE 4. Diagrams for proving the principle of the presented high-isolation building block. (a) The chassis with Ant 1 (gap-coupled loop antenna). (b) The chassis with a gap-coupled loop antenna and a half loop.

to devise a multi-antenna system (more than two antennas), additional external decoupling structure is inevitable. Therefore, it is very difficult to achieve enough stable null points on the metal ground for designing an 8 × 8 MIMO system. In this paper, the exploitation of stable null points on the ground plane's edges is set aside and a novel method is proposed.

As shown in Fig. 4(b), one can clearly see that the gap-coupled loop antenna (Ant 1) and a half loop structure are initially designed and located on the upper and lower half sections of the main system board, respectively. In this design, the half loop is meticulously devised and integrated into the chassis and its two ends are shorted to the system ground plane. During the excitation of Ant 1, two traveling waves are excited and propagate in the contrary direction along the edges of the metal ground. Notably, an additional propagation path is also introduced. By further observing Fig. 4(b), the two excited traveling waves also propagate along the half loop and thus developed a new standing-wave region, in which the stable current null points appearing in the standing wave region (on the half loop) are employed to design the other antenna. It is noteworthy that the number of the stable current null points can be determined by tuning the total length of the half loop.

Under the consideration of the building block size, in this work, only one stable current null point is to be retained by optimizing the length of the half loop. Furthermore, the position of the feeding port 2 is decided and based on the location of the stable current null point. Under this circumstance,

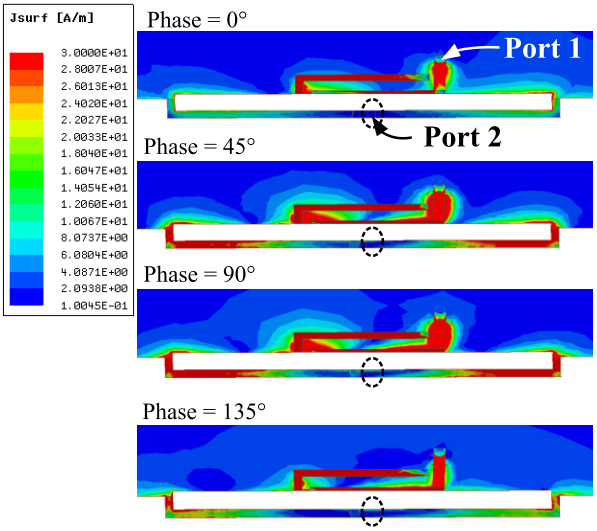

FIGURE 5. Simulated surface current distributions of the high-isolation building block with different phases at 3.5 GHz.

a loop antenna (Ant 2) is formed via the feeding of port 2 into the half loop. Eventually, the proposed building block formed by Ant 1 (gap-coupled loop antenna) and Ant 2 (loop antenna) is realized, and because port 2 is located at current null when port 1 is excited, very high isolation between the two ports is expected.

To further validate the proposed novel decoupling mechanism, the current distributions of the designed high-isolation building block with different phases (0°, 45°, 90° and 135°) during the excitation of Ant 1 are displayed in Fig. 5. In this figure, one can see that the current distributions at the feed port of the loop antenna (Ant 2) across different phases are always very small, which contributes to higher isolation.

Fig. 6 shows the simulated and measured far-field three-dimensional radiation patterns of the gap-coupled loop antenna (Ant 1) and loop antenna (Ant 2) at 3.5 GHz. In this figure, Ant 1 has exhibited maximum radiation along the z-axis, during the excitation of port 1. In contrast, during the excitation of Ant 2, the maximum radiations of the loop antenna (Ant 2) are appearing in the y-axis direction and an obvious radiation null can be seen at the ±z axis. Therefore, the radiation patterns of Ants 1 and 2 are particularly different and in orthogonal directions. Consequently, the orthogonal radiation patterns of Ant 1 and Ant 2 can guarantee high isolation and low ECC of the proposed building block. As exhibited in Fig. 6(b), the measured radiation patterns agreed well with the simulated ones, showing diversified radiation patterns for Ant 1 and Ant 2.

In summary, the main reasons for achieving high isolation and low ECC for the proposed building block are as follows; (1) The excited standing wave region of the gap-coupled loop antenna (Ant 1) is constructed on the loop antenna (Ant 2). (2) The feed point of the loop antenna is selected at the stable current null location. (3) Ant 1 and Ant 2 have exhibited orthogonal radiation pattern characteristics.

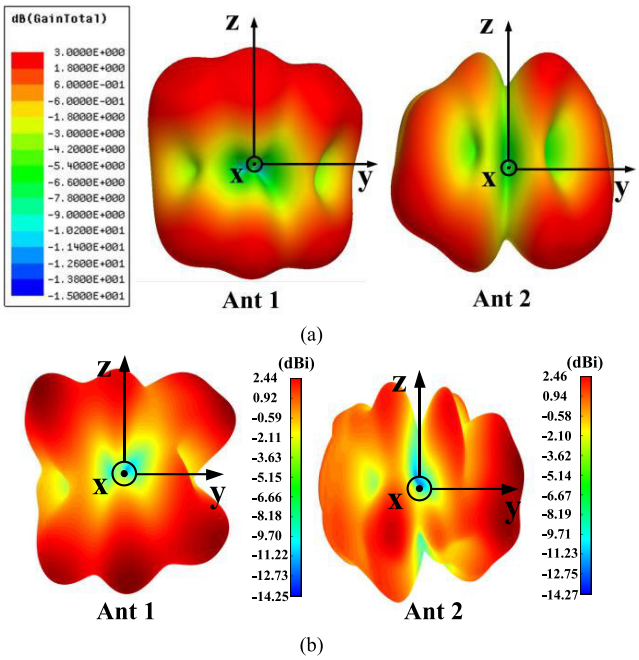

FIGURE 6. (a) Simulated and (b) measured three-dimensional radiation patterns of Ant 1 and Ant 2 at 3.5 GHz.

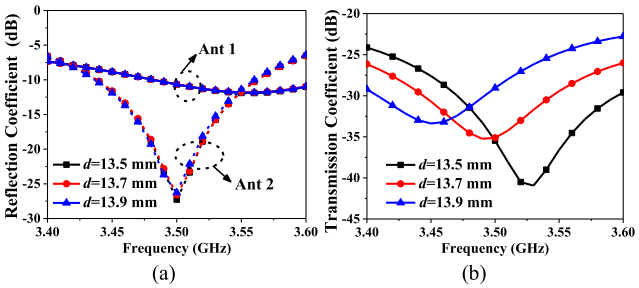

FIGURE 7. Simulated results of the presented high-isolation building block with different *d* values. (a) Reflection coefficients of Ants 1 and 2. (b) Transmission coefficients.

C. PARAMETRIC STUDY

In this sub-section, the analysis on several vital parameters is conducted. Since the stable current null excited by Ant 1 is very important to control the isolation of the proposed building block, the effects of distance d between Ants 1 and 2 on the isolation of the building block are investigated and the results are presented in Fig. 7. Here, distance d is slightly varied from 13.5 mm to 13.9 mm by shifting the position of Ant 1 (while the other parameters remain constant). As shown in Fig. 7(a), the resonant frequencies of Ants 1 and 2 remain nearly constant when tuning d. In comparison, the variation of the distance d influences the isolation of the building block significantly, as presented in Fig. 7(b). For d = 13.5 mm, the stable current null located at the feed position of Ant 2 (during Ant 1 excitation) moves to higher frequency at 3.53 GHz. In contrast, when d is increased to 13.9 mm, the stable current null located at the feed position of Ant 2 (during Ant 1 excitation) is moved to lower frequency

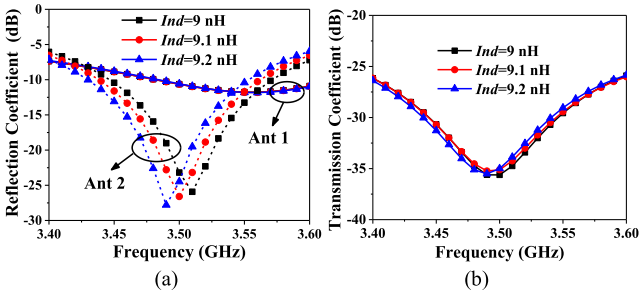

FIGURE 8. Simulated results of the presented building block as a function of the inductor values (*Ind*). (a) Reflection coefficients of Ants 1 and 2. (b) Transmission coefficients.

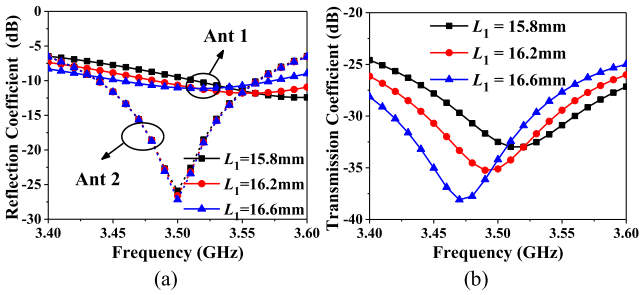

FIGURE 9. Simulated results of the presented building block as a function of the length L_1. (a) Reflection coefficients of Ants 1 and 2. (b) Transmission coefficients.

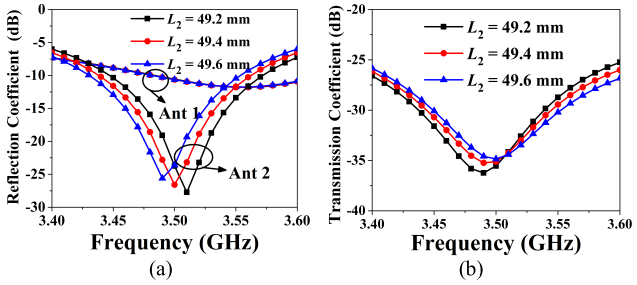

FIGURE 10. Simulated results of the presented building block as a function of the length L_2. (a) Reflection coefficients of Ants 1 and 2. (b) Transmission coefficients.

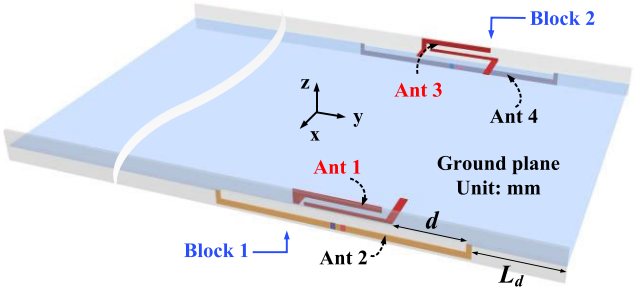

FIGURE 11. Construction of the proposed four-antenna MIMO system. $d = 13.7$, $L_d = 16.4$. (Unit: mm).

at 3.45 GHz. Finally, distance d is selected as 13.7 mm, because it can yield stable current null at near 3.5 GHz.

The effects of the series chip inductor (*Ind*) on the proposed high-isolation building block is evaluated and shown in Fig. 8. As shown in Fig. 8(a), it is apparent that the variation in *Ind* (from 9 nH to 9.2 nH) can result in shifting the resonant frequency of Ant 2 (loop antenna) to lower frequency, whereas the resonant frequency of Ant 1 almost remains unaffected. These phenomena are reasonable because the inductor is only incorporated for Ant 2. In addition, varying the inductor value has very little effect on the isolation of the proposed building block, which is due to the position of the stable current null induced by Ant 1 is very slightly shifted. Notably, the optimized *Ind* is chosen to be 9.1 nH.

To investigate the effects of tuning length L_1 of the proposed building block, the simulated results of varying L_1 from 15.8 mm to 16.6 mm are exhibited in Fig. 9. As observed in Fig. 9(a), the increase of L_1 from 15.8 mm to 16.6 mm only affects the resonant frequency of Ant 1. This is because only the electrical length of the Ant 1 is varied. Furthermore, the resonance dip of S_{21} has also shifted to the lower frequency. These phenomena are largely because the resonant frequency of Ant 1 has been changed and the position of the induced stable current null on Ant 2 is also detuned. Eventually, if the distance between the Ants 1 and 2 is adjusted, the resonance dip of S_{21} will remain at 3.5 GHz. Finally, L_1 is optimized at 16.2 mm.

To analyze the effects of varying length L_2 of the proposed building block, the simulated results of tuning L_2 from 49.2 mm to 49.6 mm are dipicted in Fig. 10. When the length L_2 is varied, the variations of the distances between the Ant 1 and the two shorted ends of the Ant 2 are the same. As seen in Fig. 10(a), the increase of L_2 from 49.2 mm to 49.6 mm only affects the resonant frequency of Ant 2. This is because only the electrical length of the Ant 2 is varied. In addition, varying L_2 has little effect on the isolation of the proposed building block, which is due to the slight variation of the position of the stable current null induced by Ant 1. Finally, the optimized L_2 is chosen to be 49.4 mm.

According to the above parametric studies, the isolation of the proposed building block is mainly dependent on the position of the induced stable current null at Ant 2. Therefore, by applying the proposed method, good decoupling between two antennas can be successfully realized with the same or different operating frequency bands.

III. MULTI-ANTENNA MIMO ARRAY

According to the provided decoupling method, a high-isolation building block has been successfully proposed, and to further verify the validity of the proposed high-isolation building block in multi-antenna systems, a four-antenna and an eight-antenna MIMO system are devised.

A. FOUR-ANTENNA MIMO ARRAY

Fig. 11 shows the four-antenna MIMO array designed by utilizing the proposed high-isolation building blocks.

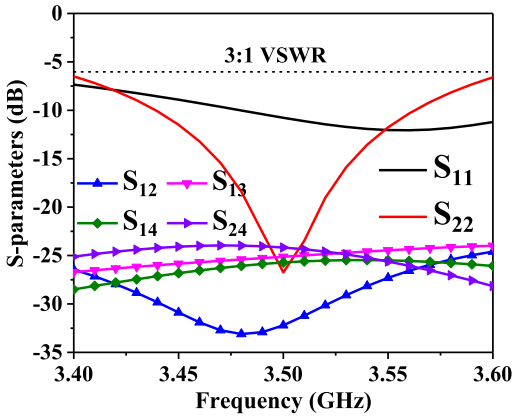

FIGURE 12. Simulated S-parameters of the proposed four-antenna MIMO system.

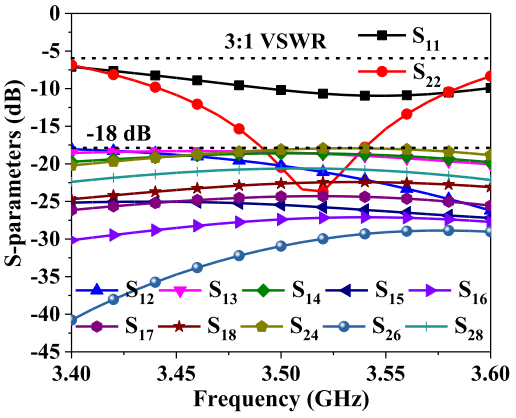

FIGURE 14. Simulated S-parameters of the proposed eight-antenna MIMO array.

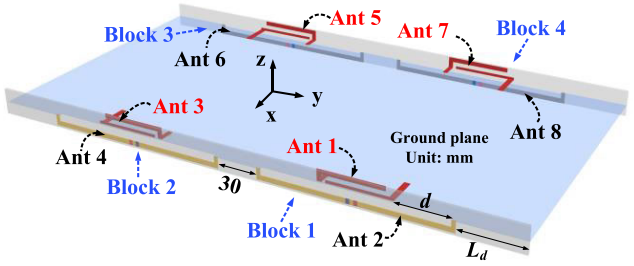

FIGURE 13. Structure of the proposed eight-antenna MIMO system. d = 13.1, Ld = 7.1. (Unit: mm).

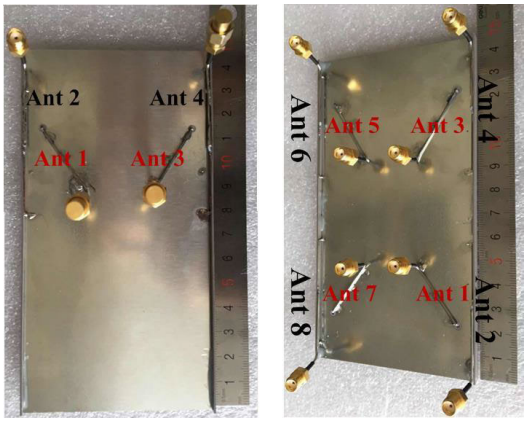

(a) (b)

FIGURE 15. Pictures of the fabricated prototypes. (a) Four-element MIMO system. (b) Eight-element MIMO system.

The detailed dimensions of the two antennas in the same building block have been discussed in Section II-A. The simulated S-parameters of the four-antenna MIMO system are presented in Fig. 12. In this figure, due to symmetrical structure, S_{33} and S_{44} are not shown for brevity, and both S_{11} and S_{22} have demonstrated impedance bandwidth better than 3:1 VSWR over the band of interest. It is noteworthy that the isolations of the four-antenna MIMO system are still better than 24 dB, which is very promising for future 5G communications.

B. EIGHT-ANTENNA MIMO ARRAY

To increase channel capacity, the proposed building block is also exploited to construct an eight-antenna MIMO system. Fig. 13 presents the symmetrical configuration of the eight-antenna MIMO system, which is formed by four identical high-isolation building blocks. Here, the distance between two building blocks of the same side board is 30 mm. For the eight-antenna MIMO array, slight modifications on d = 13.1 mm and L_d = 7.1 mm have been conducted for achieving optimized isolations, as shown in Fig. 13. The simulated S-parameters of the eight-antenna MIMO are shown in Fig. 14. In this figure, the 6-dB impedance bandwidths of the proposed eight-antenna MIMO array can well cover the desired band of interest, and its isolations are also higher than 18 dB. Notably, we cannot achieve very high isolation of >24 dB (as in four-antenna MIMO) is because of the coupling effects between the two building blocks printed on the same side board. Nevertheless, isolation >18 dB for an eight-antenna MIMO array is still very rarely reported in the recent open-literatures.

C. EXPERIMENTAL RESULTS

The pictures of the fabricated prototypes of proposed four-antenna and eight-antenna MIMO arrays are presented in Figs. 15(a) and 15(b), respectively. Here, all feeding ports of the multi-antenna MIMO systems were fed by 50 Ω semi-rigid cables. The S-parameters of the two fabricated MIMO systems were measured by a ROHDE&SCHWARZ ZNB40 vector network analyzer. During the measurement of one port, the other ports were matched with 50 Ω loads. For the two proposed MIMO arrays, only the measured reflection coefficients of Ants 1 and 2 are presented due to symmetrical structures of the two MIMO arrays. As described in Fig. 16(a), the measured reflection coefficients of the four-element MIMO system were lower than −6 dB across the band of interest and the measured isolations were better than 23 dB. In terms of the proposed 8 × 8 MIMO

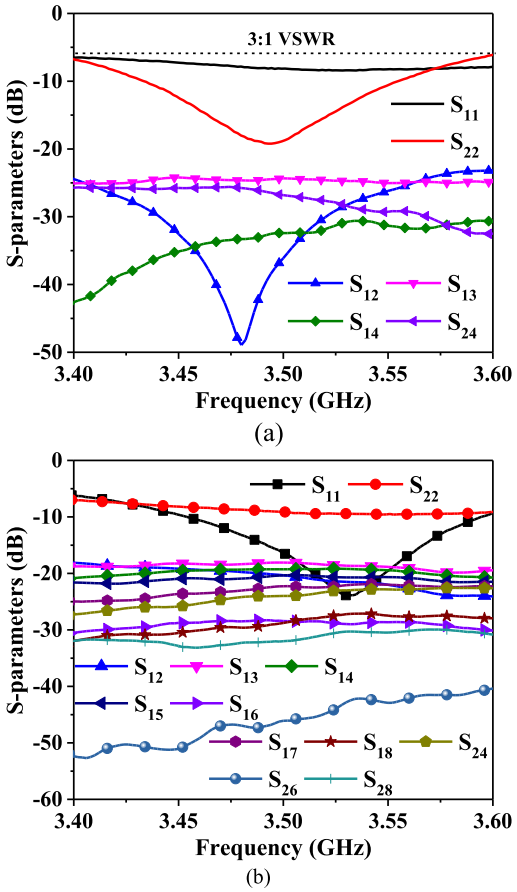

FIGURE 16. Measured S-parameters of the fabricated MIMO array prototypes. (a) Four-element MIMO system. (b) Eight-element MIMO system.

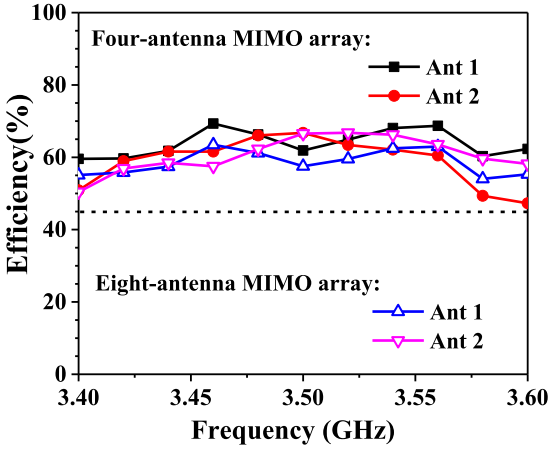

FIGURE 17. Measured efficiencies of the fabricated MIMO systems.

system, the measured 6-dB bandwidths can well cover the 3400-3600 MHz band, and measured isolations of better than 17.9 dB were also attained, as described in Fig. 16(b). Good agreements were observed between the measurement and the simulation results.

Fig. 17 exhibits the measured total efficiencies of the proposed four-antenna MIMO system and eight-antenna MIMO system. The measured total efficiencies of the 4 × 4 and

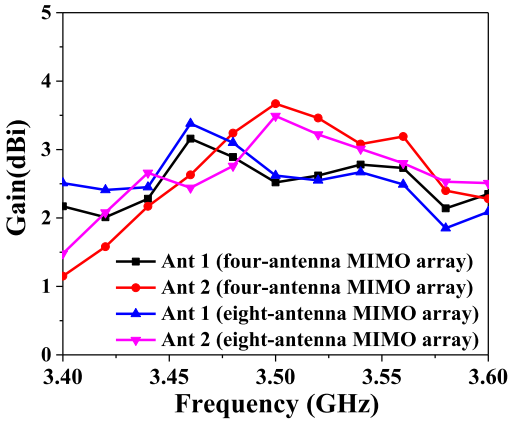

FIGURE 18. Measured peak antenna gains of the fabricated MIMO arrays.

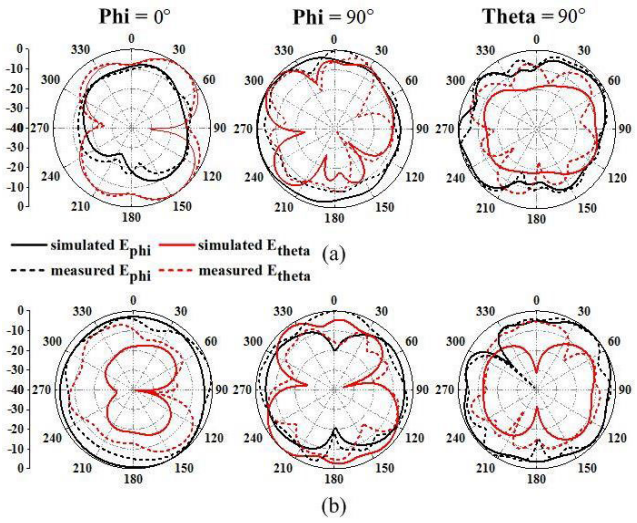

FIGURE 19. Measured and simulated normalized radiation patterns of the fabricated 8 × 8 MIMO system at 3.5 GHz. (a) Ant 1. (b) Ant 2.

8 × 8 MIMO systems were approximately 47%–69% and 50%-66%, respectively, across the band of interest. Fig. 18 shows the measured peak antenna gains of the Ant 1 and Ant 2. For the four-antenna MIMO system, across the frequency band of 3.4-3.6 GHz, the measured gains of Ant 1 and Ant 2 were varied between 1.15 and 3.67 dBi. For the eight-antenna MIMO system, the measured gains of Ant 1 and Ant 2 were approximately 1.48dBi - 3.38 dBi.

The radiation patterns of the fabricated four-antenna MIMO system and eight-antenna MIMO system were obtained in a SATIMO microwave anechoic chamber. For brevity, only the measured normalized radiation patterns of the presented eight-antenna MIMO system are given in Figs. 19(a) and 19(b), during the excitation of Ant 1 only and Ant 2 only, respectively. In these two figures, the measured radiation patterns agreed well with the simulated ones, showing diversified radiation patterns for Ant 1 and Ant 2.

D. MIMO PERFORMANCE

To verify the MIMO performances of the two proposed MIMO systems, their corresponding ECCs and channel

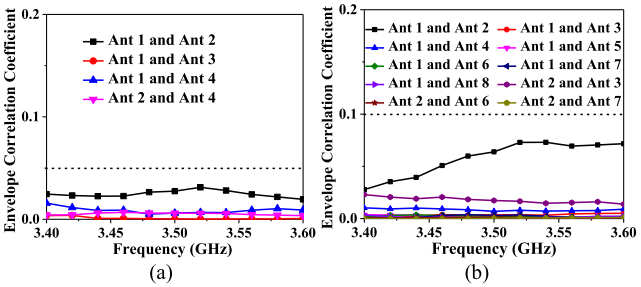

FIGURE 20. Measured ECCs of the two fabricated MIMO arrays. (a) Four-antenna. (b) Eight-antenna.

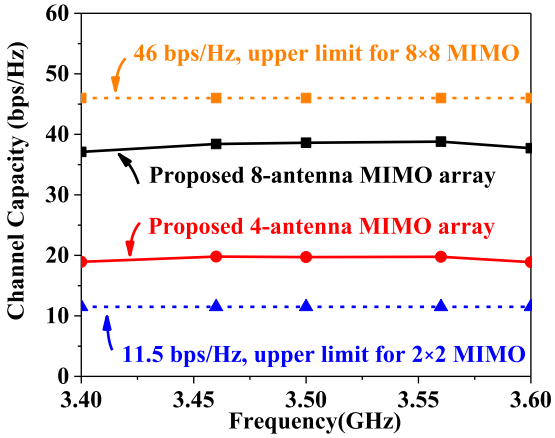

FIGURE 21. Calculated ergodic channel capacities.

capacities have been calculated and investigated. It is worth mentioning that the ECC can evaluate the pattern diversity of the different elements in a MIMO system.

The measured ECCs of the two proposed MIMO arrays are computed from the measured complex field patterns and they are plotted in Fig. 20. As shown in Fig. 20(a), across the band of interest, the ECC values of the 4 × 4 MIMO system were less than 0.032, while the measured ECCs of the fabricated 8 × 8 MIMO system were lower than 0.075, as described in Fig. 20(b). As the ECC levels of the two proposed MIMO array are far less than 0.5 (acceptable criterion for 5G MIMO antenna arrays), therefore, the proposed MIMO arrays that composed of the high-isolation building blocks have possessed good diversity performances.

The channel capacities of the fabricated MIMO systems are calculated and presented in Fig. 21. In this figure, the channel capacities of the four-antenna MIMO array are approximately 18.8-19.8 bps/Hz, which are about 1.7 times higher than the upper limit for an ideal two-antenna MIMO system (about 11.5 bps/Hz). In addition, the ergodic channel capacities of the fabricated 8 × 8 MIMO system are approximately 37.1-38.8 bps/Hz over the operation bandwidth. By comparing the ergodic channel capacities of the fabricated eight-element MIMO system with the upper limit of an eight-antenna MIMO system (with about 46 bps/Hz), it is obvious that the proposed eight-antenna MIMO array has demonstrated good

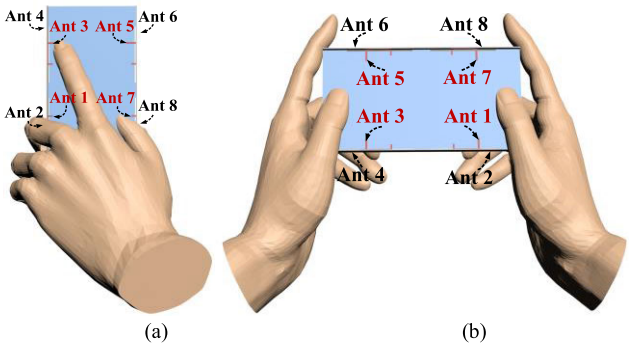

FIGURE 22. The configurations of two scenarios. (a) Single-hand operation (SH). (b) Two-hand operations (TH).

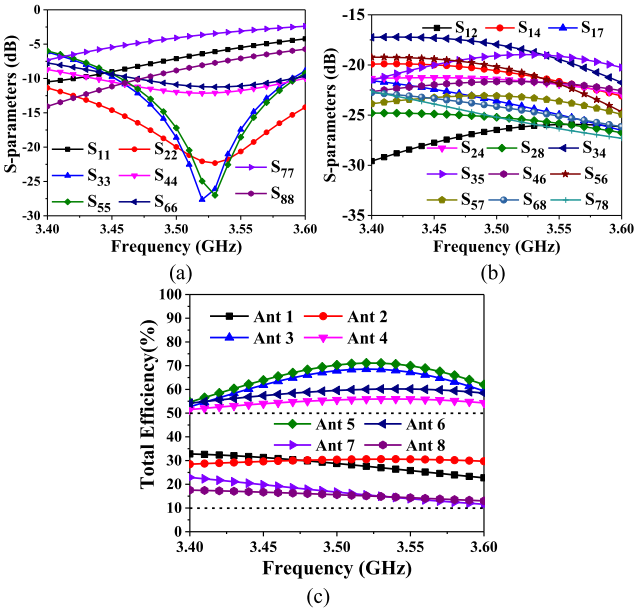

FIGURE 23. Simulated results under SH mode. (a) Reflection coefficients. (b) Transmission coefficients. (c) Total efficiencies.

channel capacities. Therefore, the presented four-antenna MIMO system and eight-antenna MIMO system can exhibit good multiplexing capability.

E. USER'S HAND EFFECT

The influences of user's hand on the presented eight-antenna MIMO array are investigated via HFSS. As the proposed MIMO array operating in the band of 3400–3600 MHz is normally applied to data mode, therefore, the head effects are not considered. In terms of hand effects, two scenarios are considered, namely, single-hand operation (SH) and two-hand (TH) operation that are described in Figs. 22(a) and 22(b), respectively.

For SH mode, the simulated S-parameters are shown in Fig. 23. In this case, the antennas located at the lower section of the smartphone (Ants 1, 7, and 8) are directly contacted by the user's hand or fingers, therefore, their impedance matchings have been deteriorated significantly, as shown

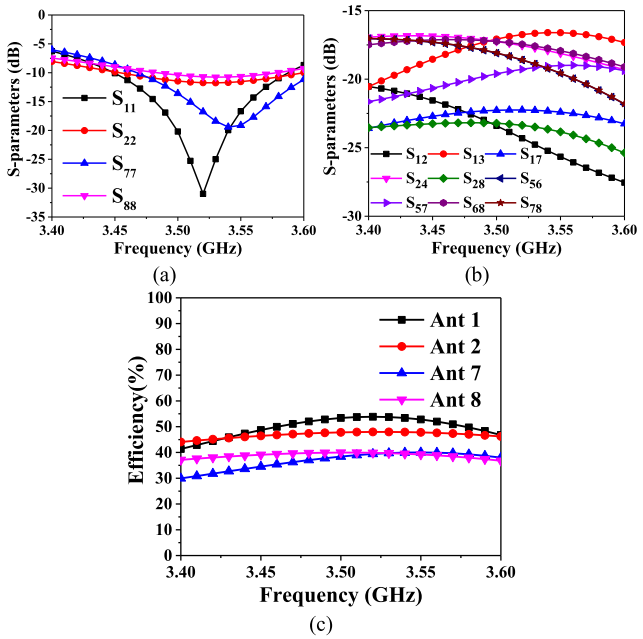

FIGURE 24. Simulated results under TH mode. (a) Reflection coefficients. (b) Transmission coefficients. (c) Total efficiencies.

TABLE 1. Comparison between the proposed MIMO arrays and the references.

Ref.	Center Freq. (GHz)	Isolation (dB)	ECC	Order
[6]	3.5	> 10	<0.2	8
[7]	3.5/5	> 11.5	<0.08/<0.05	8
[10]	2.6	> 12.5	<0.15	8
[11]	2.6	>12	<0.15	8
[12]	3.5	>12.5	<0.2	12
[13]	3.5/5.5	>11	<0.15/<0.05	10
[14]	3.5	>17	<0.07	8
[14]	3.5	>20	<0.06	4
[16]	3.5/5.5	>12	<0.15/<0.1	12
[18]	3.5	>15	<0.16	8
[21]	3.5	>13	<0.07	4
[22]	3.5	>10	<0.2	8
[23]	3.5	>17.5	<0.05	8
[24]	3.5	>25	<0.00012	2
This work 4-Ants	**3.5**	**>23**	**<0.032**	**4**
This work 8-Ants	**3.5**	**>17.9**	**<0.075**	**8**

in Fig. 23(a). Notably, good impedance matching can still be seen for Ant 2, because it is merely covered (not in physical contact with) by the middle finger. Nevertheless, the isolations between all ports are still higher than 17.2 dB, as observed in Fig. 23(b). Due to the absorption effects of the hand, Fig. 23(c) shows that the simulated total efficiencies of Ants 1, 2, 7 and 8 are lower than 35%, whereas the total efficiencies of Ants 3, 4, 5 and 6 are higher than 50%.

For TH mode, Ants 1, 2, 3 and 4 are close to the user's fingers (but not in contact), whereas Ants 5, 6, 7, and 8 are very much farther away from the user's hand, as shown in Fig. 24(b). Due to the symmetrical configuration of TH operation, for simplicity, only the results of Ants 1, 2, 7 and 8 are presented in Fig. 24. In Fig. 24(a), the reflection coefficients of Ants 1, 2, 7 and 8 are slightly affected because they are not physically touched by the user's fingers. Notably, under the consideration of TH mode, the frequency range of 3400–3600 MHz can still be covered by the proposed eight-antenna MIMO array. Similarly, their corresponding isolations are still higher than 16.8 dB, as illustrated in Fig. 24(b). From Fig. 24(c), the total efficiencies of the MIMO elements have different degrees of mitigation due to the absorption effect of user's hands or fingers, but the total efficiencies of all elements are still greater than 30%.

F. COMPARISON

Table 1 compares the performances of the proposed MIMO arrays with the other reported 5G MIMO arrays. By observing the works in [6], [7] and [10]–[13], their isolations are just between 10 dB and 12.5 dB. Compared with the work in [14], the proposed four-antenna MIMO array in this paper has exhibited better isolation of >23 dB. In addition, the measured isolation (17.9 dB) of the proposed eight-antenna MIMO in this work is also better than [14]. As for the works reported in [16], [18] and [21], [22], their attained isolations were only between 10 dB and 13 dB. Although [23] has achieved good isolation of 17.5 dB, too much space around the system ground is occupied. Furthermore, the presented eight-antenna MIMO system in this paper exhibits better isolation than [23]. By comparing the eight-antenna MIMO system size, the proposed eight-antenna MIMO system occupies the two longer sides of the system ground plane, which is comparable with the eight-element MIMO system in [6], [10] and [18]. However, the isolation of the proposed MIMO system is much better than [6], [10] and [18]. Furthermore, comparing with the reported eight-antenna MIMO systems in [13], [16] and [23], the proposed eight-antenna MIMO system has a smaller size and higher isolation. Although the reported eight-element MIMO systems in [7], [11], [12] and [22] have a smaller size, their isolations are just between 11.5 dB and 12.5 dB and the proposed eight-antenna MIMO array has much higher isolation (>17.9). Therefore, even though the size of the proposed high-isolation building block is not very compact, the eight-antenna MIMO array composed of the proposed high-isolation building blocks has an acceptable size and very desirable isolation. Although the designed two-element MIMO in [24] can achieve high isolation of better than 25dB, additional external decoupling structures are necessary to devise a multi-antenna MIMO system (more than two antennas) with the decoupling method in [24]. In addition, as the number of the excited stable null-amplitude E-field of the ground plane is also limited, the method in [24] is difficult to design a MIMO array with more than 6- or 8-antenna elements. Finally, it is noteworthy that the novel method

provided in this paper can be applied to multi-antenna MIMO systems, and the proposed multi-antenna MIMO arrays (four-antenna MIMO system and eight-antenna MIMO system) in this paper can yield high isolation without loading any additional external decoupling structure.

IV. CONCLUSION

In this paper, a novel high-isolation building block design composed of a gap-coupled loop antenna and a loop antenna has been successfully proposed, which can yield high isolation of better than 26 dB over the desired LTE band 42 (3.4–3.6 GHz). The high-isolation building block was further exploited to construct a four-antenna MIMO array and an eight-antenna MIMO array, and they have exhibited desirable isolations of better than 23 dB and 17.9 dB, respectively, without the need to load any additional external decoupling structure. The measured efficiencies of the four-antenna and eight-antenna MIMO array were 47%–69% and 50%–66%, respectively. Furthermore, desirable ECCs of lower than 0.032 and 0.075 of the proposed four-antenna and eight-antenna MIMO arrays were also calculated, respectively. User's hand effects have also been investigated in this work. From the above results, it has verified that the design method in this paper is suitable for multi-antenna systems applications and the proposed four-antenna and eight-antenna MIMO arrays are very promising for future 5G smartphone applications.

REFERENCES

[1] W. Hong, "Solving the 5G mobile antenna puzzle: Assessing future directions for the 5G mobile antenna paradigm shift," *IEEE Microw. Mag.*, vol. 18, no. 7, pp. 86–102, Nov. 2017.
[2] WRC-15 Press Release. *World Radiocommunication Conference Allocates Spectrum for Future Innovation*. Accessed: Nov. 27, 2015. [Online]. Available: http://www.itu.int/net/pressoffice/press_releases/2015/56.aspx
[3] K. L. Wong, J.-Y. Lu, L.-Y. Chen, W.-Y. Li, and Y.-L. Ban, "8-antenna and 16-antenna arrays using the quad-antenna linear array as a building block for the 3.5-GHz LTE MIMO operation in the smartphone," *Microw. Opt. Technol. Lett.*, vol. 58, no. 1, pp. 174–181, Jan. 2016.
[4] J.-Y. Lu, K.-L. Wong, and W.-Y. Li, "Compact eight-antenna array in the smartphone for the 3.5-GHz LTE 8×8 MIMO operation," in *Proc. IEEE 5th Asia–Pacific Conf. Antennas Propag. (APCAP)*, Kaohsiung, Taiwan, Jul. 2016, pp. 323–324.
[5] K.-L. Wong, C.-Y. Tsai, J.-Y. Lu, D.-M. Chian, and W.-Y. Li, "Compact eight MIMO antennas for 5G smartphones and their MIMO capacity verification," in *Proc. URSI Asia–Pacific Radio Sci. Conf. (URSI AP-RASC)*, Seoul, South Korea, Aug. 2016, pp. 1054–1056.
[6] Y.-L. Ban, C. Li, C.-Y.-D. Sim, G. Wu, and K.-L. Wong, "4G/5G multiple antennas for future multi-mode smartphone applications," *IEEE Access*, vol. 4, pp. 2981–2988, 2016.
[7] J. L. Guo, L. Cui, C. Li, and B. H. Sun, "Side-edge frame printed eight-port dual-band antenna array for 5G smartphone applications," *IEEE Trans. Antennas Propag.*, vol. 66, no. 12, pp. 7412–7417, Dec. 2018.
[8] M. Ikram, R. Hussain, A. Ghalib, and M. S. Sharawi, "Compact 4-element MIMO antenna with isolation enhancement for 4G LTE terminals," in *Proc. IEEE Int. Symp. Antennas Propag. (APSURSI)*, Fajardo, Puerto Rico, Jun./Jul. 2016, pp. 535–536.
[9] A. Ghalib and M. S. Sharawi, "TCM analysis of defected ground structures for MIMO antenna designs in mobile terminals," *IEEE Access*, vol. 5, pp. 19680–19692, 2017.
[10] M.-Y. Li, Y.-L. Ban, Z.-Q. Xu, G. Wu, C.-Y.-D. Sim, K. Kang, and Z.-F. Yu, "Eight-port orthogonally dual-polarized antenna array for 5G smartphone applications," *IEEE Trans. Antennas Propag.*, vol. 64, no. 9, pp. 3820–3830, Sep. 2016.
[11] M.-Y. Li, Z.-Q. Xu, Y.-L. Ban, C.-Y.-D. Sim, and Z.-F. Yu, "Eight-port orthogonally dual-polarised MIMO antennas using loop structures for 5G smartphone," *IET Microw., Antennas Propag.*, vol. 11, no. 12, pp. 1810–1816, 2017.
[12] M.-Y. Li, Y.-L. Ban, Z.-Q. Xu, J. Guo, and Z.-F. Yu, "Tri-polarized 12-antenna MIMO array for future 5G smartphone applications," *IEEE Access*, vol. 6, pp. 6160–6170, 2017.
[13] Y. Li, C.-Y.-D. Sim, Y. Luo, and G. Yang, "Multiband 10-antenna array for sub-6 GHz MIMO applications in 5-G smartphones," *IEEE Access*, vol. 6, pp. 28041–28053, 2018.
[14] L. B. Sun, H. Feng, Y. Li, and Z. Zhang, "Compact 5G MIMO mobile phone antennas with tightly arranged orthogonal-mode pairs," *IEEE Trans. Antennas Propag.*, vol. 66, no. 11, pp. 6364–6369, Nov. 2018.
[15] A. A. Al-Hadi, J. Ilvonen, R. Valkonen, and V. Viikari, "Eight-element antenna array for diversity and MIMO mobile terminal in LTE 3500 MHz band," *Microw. Opt. Technol. Lett.*, vol. 56, no. 6, pp. 1323–1327, Jun. 2014.
[16] Y. Li, C.-Y.-D. Sim, Y. Luo, and G. Yang, "12-Port 5G massive MIMO antenna array in Sub-6GHz mobile handset for LTE bands 42/43/46 applications," *IEEE Access*, vol. 6, pp. 344–354, 2017.
[17] L. Qu, H. Lee, H. Shin, M.-G. Kim, and H. Kim, "MIMO antennas using controlled orthogonal characteristic modes by metal rims," *IET Microw., Antennas Propag.*, vol. 11, no. 7, pp. 1009–1015, Feb. 2017.
[18] Y. Liu, A. Ren, H. Liu, H. Wang, and C.-Y.-D. Sim, "Eight-port MIMO array using characteristic mode theory for 5G smartphone applications," *IEEE Access*, vol. 7, pp. 45679–45692, 2019.
[19] J.-Y. Lu, H.-J. Chang, and K.-L. Wong, "10-antenna array in the smartphone for the 3.6-GHz MIMO operation," in *Proc. IEEE Int. Symp. Antennas Propag. USNC/URSI Nat. Radio Sci. Meeting*, Vancouver, BC, Canada, Jul. 2015, pp. 1220–1221.
[20] Z. Qin, G.-Y. Wen, M. Zhang, and J. Wang, "Printed eight-element MIMO system for compact and thin 5G mobile handest," *Electron. Lett.*, vol. 52, no. 6, pp. 416–418, Mar. 2016.
[21] Q. Chen, H. Lin, J. Wang, L. Ge, Y. Li, T. Pei, and C.-Y.-D. Sim, "Single ring slot-based antennas for metal-rimmed 4G/5G smartphones," *IEEE Trans. Antennas Propag.*, vol. 67, no. 3, pp. 1476–1487, Mar. 2019.
[22] K.-L. Wong, C.-Y. Tsai, and J.-Y. Lu, "Two asymmetrically mirrored gap-coupled loop antennas as a compact building block for eight-antenna MIMO array in the future smartphone," *IEEE Trans. Antennas Propag.*, vol. 65, no. 4, pp. 1765–1778, Apr. 2017.
[23] Y. Li, C.-Y.-D. Sim, Y. Luo, and G. Yang, "High-isolation 3.5 GHz eight-antenna MIMO array using balanced open-slot antenna element for 5G smartphones," *IEEE Trans. Antennas Propag.*, vol. 67, no. 6, pp. 3820–3830, Jun. 2019.
[24] X. Zhao, S. P. Yeo, and L. C. Ong, "Decoupling of inverted-F antennas with high-order modes of ground plane for 5G mobile MIMO platform," *IEEE Trans. Antennas Propag.*, vol. 66, no. 9, pp. 4485–4495, Jun. 2018.

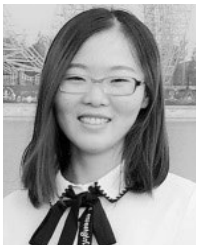

AIDI REN was born in Chaohu, Anhui, China, in 1991. She received the B.Eng. degree in electrical engineering from Xidian University, Xi'an, china, in 2014, where she is currently pursuing the Ph.D. degree. Her current research interests include small antennas for handset device and MIMO antennas for wireless communications, especially for massive MIMO antenna for future 5G smartphones.

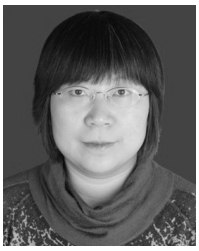

YING LIU (SM'17) received the B.Eng., M.S., and Ph.D. degrees in electromagnetics from Xidian University, Xi'an, China, in 1998, 2001, and 2004, respectively. From 2006 to 2007, she was a Postdoctoral Research with Hanyang University, Seoul Korea.

She is currently a Full Professor and the Director of the National Key Laboratory of Science and Technology on Antennas and Microwaves, Xidian University. She has authored or coauthored more than 100 refereed journal articles. She has also authored *Prediction and Reduction of Antenna Radar Cross Section* (Xi'an: Xidian University Press, 2010), and *Antennas for Mobile Communication Systems* (Beijing: Electronics Industry Press, 2011). Her research interests include antenna theory and technology, prediction, and control of antenna RCS. She is a Senior Member of the Chinese Institute of Electronics (CIE) and a Fellow of IET. She serves as an Associate Editor in IEEE Access. She was a recipient of New Century Excellent Talents in University of the Ministry of Education for China, in 2011. She is a Reviewer of several international journals and serves as TPC members or session chairs for several IEEE flagship conferences.

HONG-WEI YU was born in Xinyang, Henan, China. He received the B.Eng. degree in electrical engineering from Xidian University, Xi'an, China, in 2014, where he is currently pursuing the Ph.D. degree. His current research interests include microstrip antennas, circularly polarized antennas, and leaky-wave antennas.

YONGTAO JIA (M'18) was born in Tangshan, China, in 1989. He received the B.Eng. and Ph.D. degrees in electromagnetics from Xidian University, Xi'an, China, in 2012 and 2017, respectively. He is currently a Postdoctoral Fellow with Xidian University. His research interests include antenna radar cross-section reduction, metasurface, and wideband phased arrays.

CHOW-YEN-DESMOND SIM (M'07–SM'13) was born in Singapore, in 1971. He received the B.Sc. degree from the Engineering Department, University of Leicester, U.K., in 1998, and the Ph.D. degree from the Radio System Group, Engineering Department, University of Leicester, in 2003. From 2003 to 2007, he was an Assistant Professor with the Department of Computer and Communication Engineering, Chienkuo Technology University, Changhua, Taiwan. In 2007, he joined the Department of Electrical Engineering, Feng Chia University (FCU), Taichung, Taiwan, as an Associate Professor, where he became a Full Professor, in 2012, and as a Distinguish Professor, in 2017. He has served as the Executive Officer of Master's Program with the College of Information and Electrical Engineering (Industrial Research and Development), the Director of the Intelligent IoT Industrial Ph.D. Program, from August 2015 to July 2018. He has also served as the Director of the Antennas and Microwave Circuits Innovation Research Center, Feng Chia University, from 2016 to 2019, where he is currently serving as the Head of the Department of Electrical Engineering. He has authored or coauthored more than 140 SCI articles. His current research interests include antenna design, VHF/UHF tropospheric propagation, and RFID applications. He is a Fellow of the Institute of Engineering and Technology (FIET), a Senior Member of the IEEE Antennas and Propagation Society, and a Life Member of the IAET. He served as the TPC Member of the APMC 2012, the APCAP 2015, IMWS-Bio 2015, CSQRWC 2016, ICCEM 2017, APCAP 2018, CIAP 2018, and ISAP 2019. He was a recipient of the IEEE Antennas and Propagation Society Outstanding Reviewer Award (the IEEE Transactions on Antennas and Propagation) for six consecutive years, from 2014 to 2019. He has also received the Outstanding Associate Editor Award from the IEEE Antennas and Wireless Propagation Letters, in July 2018. He has also served as the TPC Sub-Committee Chair (Antenna) of the ISAP 2014, PIERS 2017 and PIERS 2019. He was invited as the Workshop/Tutorial Speaker in APEMC 2015, iAIM 2017, InCAP 2018, and Invited Speaker of TDAT 2015, iWAT 2018, APCAP 2018, ISAP 2019, and InCAP 2019. He was the Keynote Speaker of SOLI 2018. He has served as the Advisory Committee of InCAP 2018. He has served as the Chapter Chair of the IEEE AP-Society, Taipei Chapter, from January 2016 to December 2017. He has been the founding Chapter Chair of the IEEE Council of RFID, Taipei Chapter, since October 2017. He has also served as the TPC Chair of the APCAP 2016 and iWEM 2019. He is also serving as the General Co-Chair of ISAP 2021. He is also serving as an Associate Editor of the IEEE AWPL, IEEE Access, the IEEE Journal of RFID, and the *International Journal of RF and Microwave Computer-Aided Engineering* (Wiley). Since October 2016, he has also been serving as the Technical Consultant of SAG (Securitag Assembly Group), which is one of the largest RFID tag manufacturers, Taiwan.

YUNXUE XU received the M.S. and Ph.D. degrees in electromagnetics from Xidian University, Xi'an, China, in 2005 and 2009, respectively. He is currently an Associate Professor with the National Key Laboratory of Science and Technology on Antennas and Microwaves, Xidian University. He has authored or coauthored more than 50 refereed journal articles. He is the author of Prediction and Reduction of Antenna Radar Cross Section (Xi'an: Xidian Univ. Press, 2010). His research interests include antenna theory and technology, prediction and control of antenna RCS, and RCS calculation of complex targets.